International Specialty Conference on Cold-Formed Steel Structures

(2008) - 19th International Specialty Conference on Cold-Formed Steel Structures

Oct 14th, 12:00 AM

Generalized Beam Theory Formulation Able to Capture Load Application and Localized Web Buckling Effects

Dinar Camotim

V. M. Zeinoddini

Nuno M. F. Silva

Follow this and additional works at: https://scholarsmine.mst.edu/isccss

Part of the Structural Engineering Commons

Recommended Citation

Camotim, Dinar; Zeinoddini, V. M.; and Silva, Nuno M. F., "Generalized Beam Theory Formulation Able to Capture Load Application and Localized Web Buckling Effects" (2008). *International Specialty Conference on Cold-Formed Steel Structures*. 3.
https://scholarsmine.mst.edu/isccss/19iccfss/19iccfss-session1/3

Generalized Beam Theory Formulation Able to Capture Load Application and Localized Web Buckling Effects

Nuno M.F. Silva[1], Dinar Camotim[2] and Nuno Silvestre[3]

Abstract

This paper presents the formulation and illustrates the application of a novel Generalized Beam Theory (GBT) formulation able to handle the influence of localized effects on the buckling behavior of prismatic thin-walled members (*e.g.*, cold-formed steel profiles) – for instance, this formulation accounts for effects stemming from (i) the position of transverse loads (with respect to cross-section shear centers) or (ii) the occurrence of web buckling phenomena (*e.g.*, web crippling). In order to achieve this goal, the GBT formulation traditionally employed in buckling analyses must be enhanced by including specific (i) non-linear terms and (ii) transverse extension modes. Due to its unique modal nature and computational efficiency, this GBT formulation/implementation is a very advantageous alternative to shell finite element analyses – at present, the only available method to capture the above localized effects rigorously. In order to illustrate the application and capabilities of the proposed GBT formulation-implementation, one presents and discusses numerical results concerning the buckling behavior of (i) hat and I-section cantilevers acted by transverse tip point loads applied at various cross-section points, and (ii) I-section simply supported beams under top-flange distributed and point loads – one also assesses how end support transverse web stiffeners improve the beam buckling behavior. For validation, the GBT results are compared with values reported in the literature and/or yielded by ABAQUS shell finite element analyses.

---

[1]Ph.D. Student, [2]Associate Professor and [3]Assistant Professor, Department of Civil Engineering and Architecture, IST/ICIST, Technical University of Lisbon, Portugal.

Introduction

Due to the growing demand for structural configurations that are progressively more efficient and/or "architecturally daring" (*i.e.*, leaving a lasting aesthetic impression), steel designers have been frequently led to solutions involving extremely slender thin-walled members (*e.g.*, cold-formed steel profiles). However, optimizing the geometry of a member, thus minimizing the material expenditure and/or maximizing the visual impact, invariably renders it highly susceptible to several types of instability: global, local and *localized* buckling phenomena – the latter, which receive particular attention in this work, often stem from the existence of very slender walls (usually webs) and/or from the presence of transverse loads, which may act at different cross-section points.

It is well known that the lateral-torsional buckling behavior of thin-walled metal or FRP composite beams is strongly affected by the locations of the points of application of transversal loads acting on them – the relevant quantity is the vertical distance to the cross-section shear centers. While this effect has been properly quantified in steel beams for decades (*e.g.*, Trahair 1993), the same is not true in the case of FRP composite beams – for instance, it was only a dozen years ago that Turvey (1996) addressed this issue: he conducted an experimental, analytical and numerical investigation on the lateral-torsional buckling behavior of I-section pultruded cantilevers acted by tip point loads applied in the top flange, bottom flange and shear center. However, concerning the influence of the transverse load position on the member local-plate, distortional and/or localized buckling phenomena[2] (*i.e.*, those involving cross-section in-plane deformations), the amount of available research work is much more scarce, a statement that is particularly true for distortional buckling – to the authors best knowledge, this topic has only been addressed by (i) Gonçalves & Camotim (2004) and Gonçalves (2007), who only studied a specific problem (hat-section cantilever under acted by a tip load) using an approximate one-dimensional model, and (ii) Samanta & Kumar (2006) and Kumar & Samanta (2006), who used shell finite elements to investigate the "distortional buckling"[3] of singly symmetric I-section beams acted by transverse loads applied at their top and bottom flanges.

---

[2] Note that local-plate and distortional buckling are sometimes grouped under the designation "local buckling", characterized by the fact that the member axis remains undeformed. On the other hand, local-plate buckling is often termed "local buckling". As for distortional buckling, it may occur in members with end-stiffened lipped flanges (*e.g.*, lipped channel, hat-section or rack-section profiles) and always involves rigid body rotations of member wall assemblies – *e.g.*, a compressed flange-lip assembly rotating about the corresponding web-flange longitudinal edge).

[3] It is important to mention that this "distortional buckling" phenomenon is not the same that was described in the previous footnote (which cannot occur in I-section beams with no lipped flanges). Indeed, it is triggered by the (lateral) transverse bending and has been originally designated as "lateral-distortional buckling" by Bradford (1992) – this designation was subsequently also used by Pi and Trahair (1997), Very recently, Dinis *et al.* (2008) proposed "lateral-torsional-distortional buckling", a wording that, in their opinion, reflects more closely the mechanics of this phenomenon.

Concerning the localized buckling phenomena that stem from the high slenderness of the member walls (usually webs), they may arise in several practical applications – for instance, industrial crane girders and large-span steel or composite (steel-concrete) bridges. In both cases, the beams have virtually always very slender webs and, when acted by top-flange point loads, often experience web localized buckling phenomena, such as web crippling or shear buckling. Unlike lateral-torsional and local-plate buckling, which are rather well studied and understood phenomena, is it fair to say that there are practically no simplified (one-dimensional) models to assess, with reasonable accuracy, instabilities stemming from transverse normal and/or shear stresses – indeed, the few available models either (i) are of a semi-empirical nature and exhibit a low and somewhat unpredictable accuracy (*e.g.*, the design formulae and methodologies prescribed by most of the current steel codes, such as the very recently published Part 1-5 of Eurocode 3 – CEN 2006), or (ii) have a limited range of application (*e.g.*, cannot handle buckling mode coupling effects). Therefore, it is not surprising that nearly all the works reported on localized buckling phenomena in thin-walled members (mostly involving I-beam webs) concern experimental and/or shell finite element numerical simulations. In this context, it is worth mentioning two recent publications: (i) the experimental study carried out by Lucic & Scepanivic (2004), dealing with web crippling of transversally stiffened I-section beams acted by transverse loads applied eccentrically with respect to the web plane, and (ii) the numerical investigation conducted by Topkaya (2006), who analyzed the buckling behavior of simply supported I-beams with laterally restrained compression flanges. The latter provided evidence that such I-beams may exhibit a critical buckling mode that combines lateral-torsional and web local-plate buckling features – moreover, the author (i) performed a parametric study and, on the basis of the results obtained, (ii) developed semi-empirical formulae to estimate the critical loads/stresses associated with this "mixed" buckling mode.

Despite the fairly intense research activity currently going on in this area, steel designers are not yet equipped with numerical tools allowing them to assess efficiently and rigorously the localized web buckling behavior in thin-walled members with arbitrary loadings and support conditions. Indeed, they must either (i) use the semi-empirical design formulae and methodologies prescribed by the steel codes or (ii) resort to rather complex shell finite element analyses – this last option is very time consuming (besides the computational needs, one must not also forget the laborious data input and result interpretation) and clearly incompatible with the current design office practice in routine applications.

Recently, a novel approach to analyze the local and global buckling behavior of prismatic thin-walled members has been explored and shown to constitute a very attractive/advantageous alternative to the shell finite element modeling – this approach is based on the Generalized Beam Theory (GBT), which may be seen as a beam (one-dimensional) theory that (i) incorporates local (in-plane cross-section) deformations

and (ii) exhibits very convenient modal features. By expressing the member deformed configuration (or buckling mode shape) as a combination of *deformation modes* with clear structural meanings (local-plate, distortional and global modes), GBT provides elegant, rigorous and computationally efficient solutions for several structural problems concerning prismatic thin-walled members (*e.g.*, Camotim *et al.* 2004, 2006a, 2006b, and Bebiano *et al.* 2007) – these solutions include the majority of the (geometrically) linear and non-linear effects captured by the shell finite element analyses, but at a much lower computational cost.

The aim of this paper is (i) to present main steps involved in the formulation and implementation, and (ii) illustrate the application of a GBT-based beam finite element that incorporates non-linear terms stemming from the presence of pre-buckling normal (longitudinal and transverse) and shear stresses. This makes it possible to capture (i) the influence of the location of a transverse load point of application[4] and also (ii) localized wall (web) buckling effects. The illustrative numerical results presented and discussed concern the buckling behavior of (i) hat and I-section cantilevers acted by transverse tip point loads applied at various cross-section points, and (ii) I-section simply supported beams under top-flange distributed and point loads (*i.e.*, highly prone to web crippling) – one also assesses how the inclusion of end support transverse web stiffeners improve the beam buckling behaviour. In order to provide validation for the proposed approach and, at the same time, offer a better grasp of its capabilities, the GBT-based results are compared with values yielded by shell finite element analyses carried out in the code ABAQUS (HKS 2002).

Fundamental GBT Equations

Consider the arbitrary thin-walled prismatic member shown in figure 1, where *x*, *s* and *z* are local coordinates along the longitudinal direction (member axis), cross-section mid-line and the wall thickness – $u(x,s)$, $v(x,s)$ and $w(x,s)$ are the corresponding member mid-surface displacement fields. The key GBT feature is the fact that these displacement components are expressed by means of a linear combination of *cross-section deformation modes* – *i.e.*, one has

$$u(x,s) = u_k(s)\phi_{k,x}(x) \quad v(x,s) = v_k(s)\phi_k(x) \quad w(x,s) = w_k(s)\phi_k(x) \ , \quad (1)$$

---

[4] As mentioned earlier, Gonçalves & Camotim (2004) and Gonçalves (2007) also used GBT to study the influence of the location of a tip transverse load point of application point on the distortional and lateral-torsional buckling behaviour of hat-section cantilevers. Although the approximate methodology adopted by these authors proved to be adequate to analyse this particular problem (as far as anti-symmetric distortional and lateral-torsional buckling are concerned), it lacks generality – *e.g.*, the symmetrical distortional and local-plate buckling behaviours of these same hat-section cantilevers are not handled properly (the web in-plane rotations are no longer rigid-body ones, due to significant transversal bending).

where $u_k(s)$, $v_k(s)$ and $w_k(s)$ ($k=1,..,n$) are deformation mode shapes and $\phi_k(x)$ functions providing the longitudinal variation of their amplitudes. The cross-section deformation modes may be either (i) global (axial extension, major/minor axis bending and torsion), (ii) local (distortional and local-plate), (iii) (warping) shear or (iv) transversal extension ones − moreover, they are determined by means of a GBT "trademark"
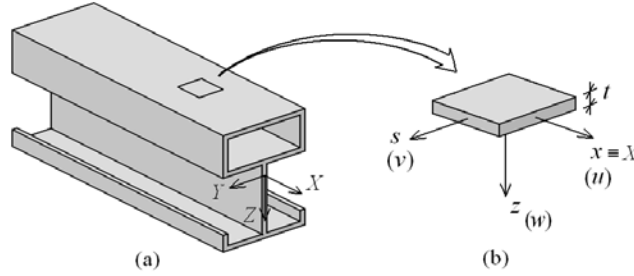

Fig. 1: (a) Geometry and (b) local coordinate system and corresponding displacement field and local of an arbitrary thin-walled cross-section

procedure termed *cross-section analysis*. The concepts and operations involved in this procedure, which are not addressed here, can be found in a very recent paper by the authors (Silva *et al.* 2008) − similar (but not identical) procedures have also been proposed by other authors, namely Silvestre & Camotim (2002) and Gonçalves (2007).

Assuming that the member is made of a material with linear elastic constitutive law, it is possible to derive the GBT equations governing its first order and buckling behaviors − they are given by

$$
\begin{aligned}
&C_{ik}\phi_{k,xxxx} + \left(E_{ik} + E_{ki} - D_{ik}\right)\phi_{k,xx} + B_{ik}\phi_k - \\
&- \lambda\left(C_{jik}\left(\phi_{j,xx}^0\phi_{k,x}\right)_{,x} + D_{jik}\left(\phi_{j,x}^0\phi_k\right)_{,x} - D_{jki}\phi_{j,x}^0\phi_{k,x} - B_{jik}\phi_j^0\phi_k\right) - q_i = 0 \quad , \quad (2)
\end{aligned}
$$

where (i) the second-order tensors (matrices) C_{ik}, B_{ik}, D_{ik} and E_{ik} account for the linear stiffness values associated with (i_1) longitudinal extensions, (i_2) transverse extensions, (i_3) shear strains and (i_4) coupling between longitudinal and transverse extensions due to Poisson effects[5], and (ii) the third-order tensors C_{jik}, B_{jik} and D_{jik} take into consideration the member geometric stiffness and concern the works done by the (ii_1) longitudinal normal, (ii_2) transverse normal and (ii_3) shear stresses, corresponding to the non-linear terms of the longitudinal extensions $\varepsilon_{xx}^{NL} = \left(v_{,x}^2 + w_{,x}^2\right)/2$, transverse extensions ($\varepsilon_{ss}^{NL} = w_{,s}^2/2$) and shear strains ($\gamma_{ss}^{NL} = w_{,x}w_{,s}$). The components of these second and third-order tensors are given by the expressions

---

[5] The tensor components E_{ik} should not be confused with the material Young's modulus E.

$$C_{ik} = \frac{E}{1-v^2} \int_b \left(tu_i u_k + \frac{1}{12} t^3 w_i w_k \right) ds$$

$$B_{ik} = \frac{E}{1-v^2} \int_b \left(tv_{i,s} v_{k,s} + \frac{1}{12} t^3 w_{i,ss} w_{k,ss} \right) ds$$

$$D_{ik} = G \int_b \left(t \left(u_{i,s} + v_i \right)\left(u_{k,s} + v_k \right) + \frac{1}{3} t^3 w_{i,s} w_{k,s} \right) ds \tag{3}$$

$$E_{ik} = \frac{vE}{1-v^2} \int_b \left(tu_i v_{k,s} + \frac{1}{12} t^3 w_i w_{k,ss} \right) ds$$

$$C_{jik} = \frac{E}{1-v^2} \int_b \int_t \left(u_j - zw_j \right)\left(v_i v_k + w_i w_k \right) dz ds$$

$$B_{jik} = \frac{E}{1-v^2} \int_b \int_t \left(v_{j,s} - zw_{j,ss} \right) w_{i,s} w_{k,s} \, dz ds \qquad . \tag{4}$$

$$D_{jik} = G \int_b \int_t \left(u_{j,s} + v_j - 2zw_{j,s} \right) w_i w_{k,s} \, dz ds$$

Finally, a vector q_i component represents the work per unit length done by a distributed load having components q_x, q_s and q_z (deemed to be applied at the wall mid-surfaces) and associated with deformation mode i – thus, one has

$$q_i = \int_b \left(q_s v_i + q_z w_i - q_{x,x} u_i \right) ds \qquad . \tag{5}$$

As mentioned above, system (2) provides the equilibrium equations governing the member first-order and buckling behaviors – they are obtained by assigning null values to either (i) the load parameter λ (first-order behavior) or (ii) the vector q_i components (buckling behavior). One should still mention that, when calculating the third-order tensor (geometric stiffness) components, the inclusion of the pre-buckling stresses and deformations effects is accomplished by means of the modal amplitude functions ϕ_j^0 (see (2)). These pre-buckling stresses (i) are the solution of the member first-order analysis under a reference loading profile (loading profile multiplying the load parameter λ in buckling analyses), and (ii) include the transverse normal stresses that appear when the loads are not applied at the cross-section shear center[6] – they may be compressive or tensile, depending on whether the load is applied above or below this shear center.

---

[6] Indeed, this is precisely the effect that this work aims at investigating.

GBT-Based Finite Element Solutions

The member first-order and buckling analyses are performed by means of GBT-based beam finite element formulations, which are similar to the one originally developed by Silvestre & Camotim (2003), in the context of the buckling analysis of pultruded FRP columns. The following strategy is adopted to approximate (discretize) the modal amplitude functions $\phi_i(x)$: (i) the functions concerning deformation modes involving non-null transverse displacements $v_i(s)$ and/or $w_i(s)$ are approximated by means of Hermite cubic polynomials, and (ii) those related with deformation modes involving only axial displacements $u_i(s)$ (*i.e.*, the axial extension and shear modes) are approximated using linear Lagrange polynomials. The corresponding element linear and geometric stiffness matrices are given by

$$
\begin{aligned}
K^e_{ik\alpha\beta} = {} & C_{ik} \int_{L_e} \psi_{\alpha,xx}\psi_{\beta,xx}dx + B_{ik}\int_{L_e}\psi_\alpha\psi_\beta dx + D_{ik}\int_{L_e}\psi_{\alpha,x}\psi_{\beta,x}dx \\
& + E_{ik}\int_{L_e}\psi_{\alpha,xx}\psi_\beta dx + E_{ki}\int_{L_e}\psi_\alpha\psi_{\beta,xx}dx
\end{aligned}
\tag{6}
$$

$$
\begin{aligned}
G^e_{ik\alpha\beta} = {} & \left(C_{jik}\int_{L_e}\psi_{\eta,xx}\psi_{\alpha,x}\psi_{\beta,x}dx + B_{jki}\int_{L_e}\psi_\eta\psi_\alpha\psi_\beta dx + \right. \\
& \left. D_{jik}\int_{L_e}\psi_{\eta,x}\psi_{\alpha,x}\psi_\beta dx + D_{jki}\int_{L_e}\psi_{\eta,x}\psi_\alpha\psi_{\beta,x}dx \right) d^0_{j\eta}
\end{aligned}
\quad , \tag{7}
$$

where (i) subscripts i, j, k identify the deformation modes, (ii) subscripts α, β concern the $\phi_i(x)$ approximation nature (Hermite/Lagrange polynomials) and (iii) $d^0_{j\eta}$ are the pre-buckling generalized displacement components – the latter are obtained through the finite element solution of the first-order problem

$$
\mathbf{d}^0 = \mathbf{K}^{-1}\mathbf{f}^0 \quad , \tag{8}
$$

where $\mathbf{K}$ and $\mathbf{f}^0$ are the member overall linear stiffness matrix and load vector. Finally, a member buckling analysis involves solving the eigenvalue problem

$$
\left(\mathbf{K} - \lambda\mathbf{G}\right)\mathbf{d} = 0 \quad , \tag{9}
$$

where vector $\mathbf{d}$ assembles the (discretized) degrees of freedom.

It is still worth pointing out that the GBT analyses required to solve the above first-order and buckling problems do not necessarily have to involve the same sets of deformation modes. For instance, very often one does not need to include shear and transverse extension modes in the buckling analyses. On the other hand, the inclusion of such deformation modes in the first-order analyses is absolutely crucial to obtain precise pre-buckling generalized displacement components $d^0_{j\eta}$ – they are then used to

evaluate "exact" pre-buckling stresses, which play a key role in determining accurate geometric stiffness values.

Illustrative Examples

In this section one presents and discusses numerical results that illustrate the application and potential of the developed GBT formulation – all are elastic buckling problems. The first two problems concern simply supported I-beams with slender webs are intended to (i) illustrate the various types of buckling phenomena that may occur in the presence of transverse loadings (applied at the top flange), (ii) assess the (beneficial) effect of adding end support transverse web stiffeners and (iii) validate the proposed GBT model, by comparing its results with ABAQUS shell finite element values. The last two problems concern the effect of the position of load point of application point on the buckling behavior of I-section and hat-section cantilevers – in this case, the GBT-based results are validates through the comparison with values (i) reported by Bebiano *et al.* (2007), for the I-section cantilevers, and (ii) again yielded by ABAQUS shell finite element analyses, for the hat-section cantilevers.

Simply Supported I-Beams. The first two illustrative examples concern simply supported beams[7] made of S460 steel ($E=210\,GPa$, $v=0.3$, $f_{yk}=460\,MPa$) and exhibiting the I-section geometry depicted in figure 2(a). They are acted by two transverse loadings applied at the top flange: either (i) two point loads (*i.e.*, distributed over a very small area, to be more precise) or (ii) a uniformly distributed load along the whole beam span. It is worth noting that, due to the high web slenderness, this cross-section is classified as "Class 4" according to Eurocode 3 (CEN 2005) – this implies that the beam ultimate strengths are strongly influenced by the occurrence of web-triggered local and/or localized buckling phenomena. For the discretization shown in figure 2(b), the GBT cross-section analysis leads to *30* deformation modes: global (**1**-**4**), local-plate (**5**-**12**), shear (**13**-**21**) and transverse extension (**22**-**30**) modes[8] – the main features of the most relevant of them are displayed in figure 3[9].

First, one analyzes the beam schematically depicted in figure 4, (i) with length *L=200 cm*, (ii) with the simple supports located in the bottom flange and (iii) acted by two symmetric vertical point loads applied at the top flange and in

---

[7] The end cross-sections can deform freely, since only the web-flange corner displacements are restrained – thy are strictly necessary to avoid cross-section rigid-body motions (global modes).

[8] All deformation modes are normalized to exhibit unit maximum displacement components – either (i) v or w (if they are not both null) or (ii) u (if v and w are both null).

[9] Recall that the shear and transverse extension deformation modes only have to be included in the member first-order analyses.
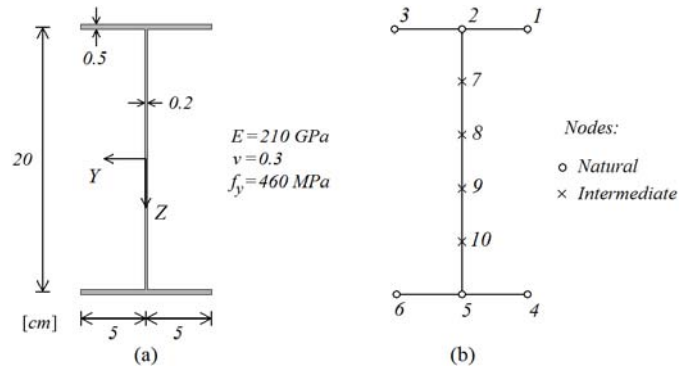
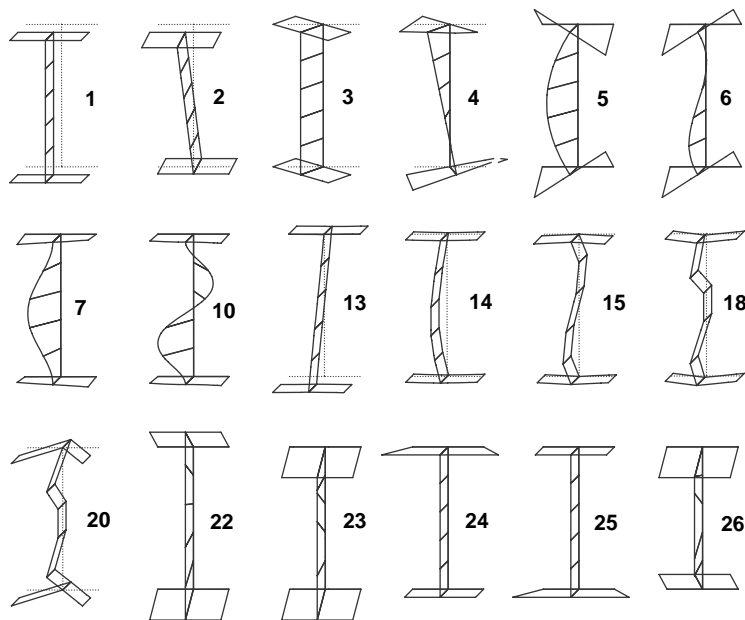Fig. 2: I-section (a) geometry and dimensions, and (b) GBT nodal discretization

Fig. 3: Main features of the most relevant I-section deformation modes: global (**1-4**),
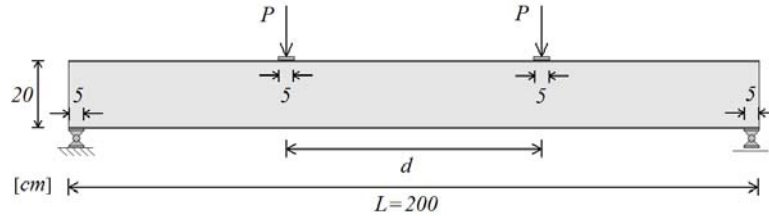local-plate (**5-12**), shear (**13-21**) and transverse extension (**22-30**)

Fig. 4: Simply supported I-section beam acted by two symmetric point loads

the plane of web – their points of application are a (variable) distance *d* apart. One assumes that (i) the point loads are effectively uniformly distributed over a length *s=5 cm* (see fig. 4) (ii) the beam is only laterally restrained at the top and bottom flanges of the end cross-sections (supports), and (iii) the flange displacements are free along the whole beam length. Concerning the presence of web transverse stiffeners, one addresses two cases: (i) no stiffeners and (ii) stiffeners only at the beam end cross-sections – each stiffener is formed by two steel plates of thickness *t_s=5 mm*, normal to the web and connecting the two flanges along their full widths.

GBT-based analyses are employed to assess the variation of the critical loadings *P_cr* with the parameter *d/L* (normalized distance between the two point loads), both for beams with and without web transverse stiffeners at the supports – all *30* deformation modes are included in the analyses[10] and the beams are discretized into *22* finite elements with different lengths (smaller in the vicinity of the supports, as can be seen in figs. 7(a) and 7(c)), which corresponds to a total of *1143* degrees of freedom (d.o.f.). For validation purposes, one also performs shell finite element analyses in the code ABAQUS – the beams are discretized into fine meshes involving *1280* S9R5 elements (9-node shell elements with *5* d.o.f. per node and reduced integration), which corresponds to an overall amount of about 27000 d.o.f.. The numerical results are presented in figures 5, 6(a)-(b) and 7(a)-(d): (i) *P_cr vs. d/L* curves, yielded by the GBT and ABAQUS analyses, (ii) GBT modal participation diagrams providing the variation, with *d/L*, of the deformation mode contributions to the beam critical buckling modes and (iii) the GBT and ABAQUS critical buckling mode shapes concerning the beams with *d/L=0.3*. The observation of these results prompts the following comments:

(i) As expected, the unstiffened beam instability is always triggered by the buckling of the web near the supports (see fig. 7(a)), due to the combined action of shear and transverse normal stresses. Obviously, this means that *P_cr* does not depend on *d/L* (provided that the loads are not applied in the close vicinity of the

---

[10] As mentioned earlier, it will be shown that the shear and transverse extension deformation modes do not participate in the beams critical buckling modes, which means that they can be omitted from the buckling analyses. Their role is restricted to the first-order analyses.

supports) − therefore, it is not surprising that the critical load remains practically constant ($P_{cr}≈17\,kN$) up to $d/L=0.8$, and then gradually decreases to about half that value ($P_{cr}=8.46\,kN$ for $d/L=1$). For $d/L=0.3$ ($P_{cr}=16.98\,kN$) all the contributions to the beam critical buckling mode come from local-plate and global deformation modes: **7** (*50%*), **5** (*30.6%*), **4** (*8%*), **10** (*5.6%*), **6** (*3.5%*) and **3** (*1.9%*)[11].

(ii) Again as expected, the stiffened beam instability is also triggered by the buckling of the web, but now in the regions where the loads are applied (see fig. 7(c)). This explains why P_{cr} decreases monotonically as the two
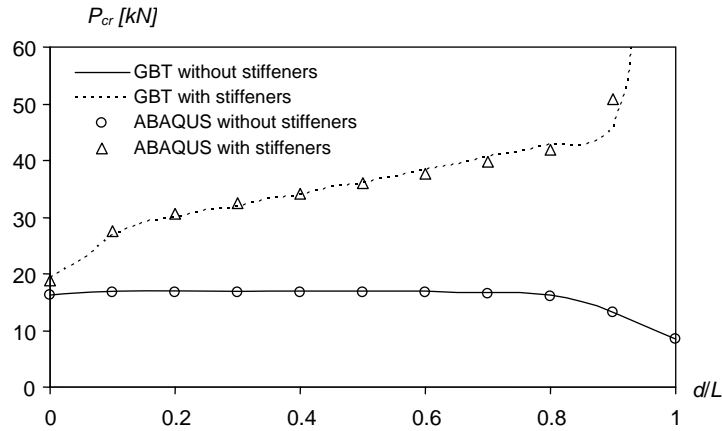
Fig. 5: P_{cr} *vs. d/L* curves for the unstiffened and stiffened I-beams

---

[11] The participations of the GBT deformation modes in the beam critical buckling mode are obtained from the maximum values, along the beam length, of the various modal amplitude functions (*e.g.*, Silva *et al.* 2008) − thus, each deformation mode contribution is expressed as a percentage value p_i. To have all deformation mode amplitudes with the same dimensions, the torsion mode one corresponds to the maximum displacement component causes by it (like for all other modes) − note that the "usual" torsion mode amplitude corresponds to a rotation value.
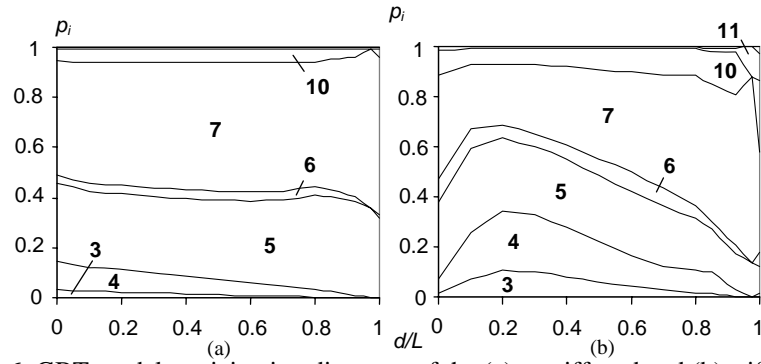
Fig. 6: GBT modal participation diagrams of the (a) unstiffened and (b) stiffened I-beams
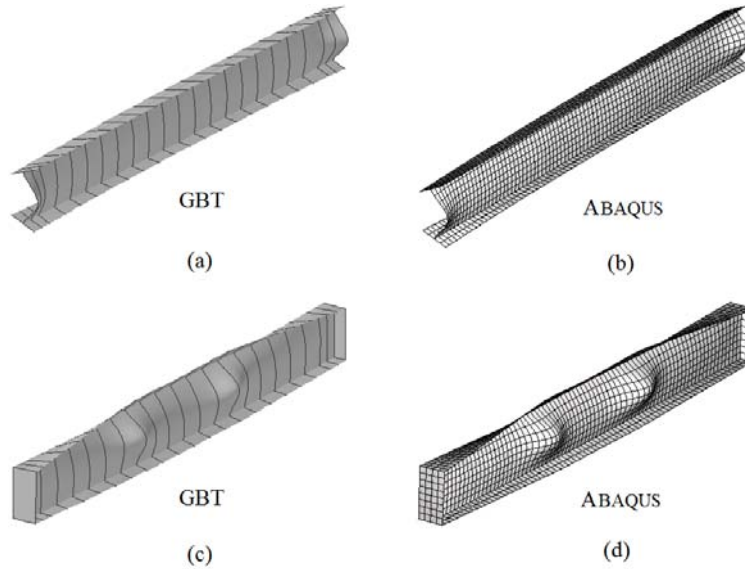

Fig. 7: Critical buckling mode shapes provided by the GBT and ABAQUS analyses for the (a+b) unstiffened and (c+d) stiffened beams with *d/L=0.3*

loads get closer (*i.e.*, as *d/L* decreases) − the lower and higher values are *19.67 kN* (mid-span loading) and *170.28 kN* (support loading). For *d/L=0.3* (P_{cr}=*32.01 kN*), the critical buckling mode combines relevant participations

from local-plate and global deformation modes: **5** (*27.5%*), **7** (*27.5%*), **4** (*22.8%*), **3** (*9.9%*), **10** (*6.3%*) and **6** (*5%*)[12].

(iii) The presence of the end web stiffeners obviously improves the beam buckling behavior − this improvement becomes more relevant as the loads get closer to the supports (unlike in the unstiffened beams, the stiffened beam P_{cr} value grows exponentially as *d/L* tends to *1*). The percentage difference between the critical buckling loads of the two beam (iii$_1$) is of *18%* for *d/L=0* and (iii$_2$) increases rapidly with *d/L − e.g.*, for *d/L=0.3* this difference is already equal to *89%*.

(iv) The GBT modal participation diagrams shown in figures 6(a)-(b) provide in-depth insight into the beam buckling behavior. For instance, they readily reveal that (iv$_1$) the global deformation modes **3** and **4** are much more important in the stiffened beams than in the unstiffened ones, (iv$_2$) the local-plate deformation modes **5** and **7** always prevail (regardless of the load position), particularly in the unstiffened beams, and (iv$_3$) the maximum global (flexural-torsional) contribution to the critical buckling mode occurs for the stiffened beam with *d/L=0.2*.

(v) Finally, note the very good agreement between the GBT and ABAQUS results − as clearly shown in figures 5 and 7, there is a virtually perfect match between both the critical load values and the buckling mode shapes, as long as one has *d/L≤ 0.8*. Indeed, the P_{cr} differences never reach either *1.2%* (unstiffened beams) or *3.0%*, (stiffened beams). For *d/L>0.8*, on the other hand, these differences may be as high as *10%*, which is due to the GBT web stiffener modeling[13]. In order to illustrate the above statements, one presents next some critical load values provided by the ABAQUS and GBT analyses for the unstiffened and stiffened beams with *d/L=0.3*: (v$_1$) $P_{cr.GBT}$=*32.01 kN* and $P_{cr.ABQ}$=*32.40 kN* (stiffened beam) and (v$_2$) $P_{cr.GBT}$=*16.97kN* and $P_{cr.ABQ}$=*16.79kN* (unstiffened beam).

The second beam analyzed differs from the first one (depicted in fig. 4) in the fact that the loading consists now of a uniformly distributed load spanning the whole member length and applied at the beam top flange (in the plane of the web) − its value is *p=2P/L*, which leads to support reactions equal to *P*. The GBT and ABAQUS critical buckling loads of the unstiffened and stiffened beams are given in table 1. In order to assess the relevance of including the non-linear term of the transverse extensions ($\varepsilon_{ss}^{NL} = w_{,s}^2/2 -$ see B_{jik} in (4)) in the buckling analysis of beams with slender

---

[12] The participation of the global modes are now much more relevant, since the cross-sections that are most involved in the beam critical buckling mode critical are located far away from the supports − thus, they exhibit a considerably smaller "global stiffness".

[13] In GBT, the web stiffeners are modeled by restraining the local-plate and transverse extension mode amplitudes in the beam end cross-sections − this corresponds to assuming that the stiffening plates are fully rigid in their own-planes and completely flexible out of them, which does not correspond to the ABAQUS shell finite element modeling. Additionally, GBT does not take into account the stresses developing in the stiffeners, thus making it impossible to capture their own (localized) buckling behaviors.

webs acted by transverse loads, table 1 also contains P_{cr} values obtained from GBT analyses that neglect this term. As for figures 8(a)-(d), they show the two beam critical buckling mode shapes yielded by GBT and ABAQUS analyses. Finally, figure 9 displays the pre-buckling shear and transverse normal stresses obtained from first-order analyses carried out in ABAQUS. After observing these results, one is led to the following conclusions:

(i) As before, the unstiffened beam instability is triggered by the buckling of the web near the supports (see fig. 8(a)). It occurs for $P_{cr}=16.16\,kN$, *i.e.*, practically the same critical buckling load of the beam acted by point loads applied far away from the supports – this is not surprising, since the critical buckling load is governed by the support reaction value, which is the same in both cases. Concerning the beam critical buckling mode, the participations of the various GBT deformation modes also attest the enormous similarity with the previous one, easily confirmed by looking at figures 8(a) and 7(a) – indeed, the main contributions come from modes **7** (*52.6%*), **5** (*32.4%*), **10** (*5.3%*), **4** (*4.8%*), **6** (*3.6%*) and **3** (*0.8%*), *i.e.*, practically the same as before.

(ii) When the transverse extension non-linear term is neglected, the GBT analysis of the unstiffened beam yields $P_{cr}=64.73\,kN$, a value four times higher than the correct one. Moreover, the participations of global modes in the beam critical buckling mode become considerably higher – the main contributions come are now from modes **7** (*27.3%*), **4** (*22.8%*), **5** (*18.8%*), **3** (*14.2%*), **10** (*8.3%*), **6** (*7.4%*) and **11** (*0.9%*).

(iii) Localized web buckling no longer occurs in the stiffened beam, given the absence of point loads – buckling now takes place in a mode that (iii$_1$) combines global deformation modes (minor axis bending and torsion) with web-governed local-plate ones, and (iii$_2$) extends throughout the

Table 1: P_{cr} values of the I-beams acted by uniformly distributed loads

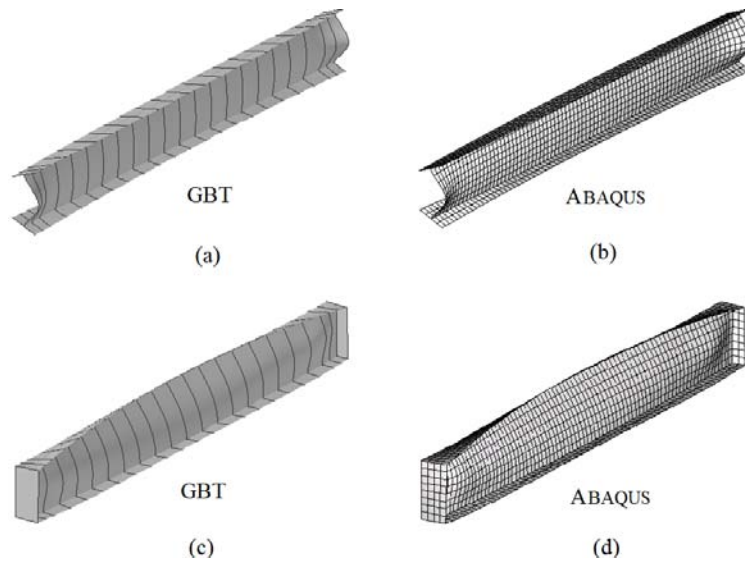| Beam	$P_{cr.ABQ}$ [kN]	$P_{cr.GBT}$ [kN]	Δ (%)	$P_{cr.GBT}$ without ε_{ss}^{NL} [kN]	Δ (%)
without stiffeners	*15.98*	*16.16*	*+1.1*	*64.73*	*+305.1*
with stiffeners	*55.88*	*53.69*	*–3.9%*	*84.40*	*+51.0*

Fig. 8: GBT and ABAQUS critical buckling mode shapes for the (a+b) unstiffened
and (c+d) stiffened beams under uniformly distributed loads

whole beam length (see fig. 8(c)). One has $P_{cr}=53.69\,kN$ and the most relevant
critical buckling mode contributions come from deformation modes **4** (*40.7%*),
3 (*20.8%*), **7** (*16%*), **5** (*15.7%*), **10** (*3.5%*) and **6** (*2.7%*).

(iv) When the transverse extension non-linear term is neglected, the GBT analysis of
the stiffened beam yields $P_{cr}=84.40\,kN$, which corresponds to a *57%* increase with
respect to the correct value. As for the deformation mode contributions to the
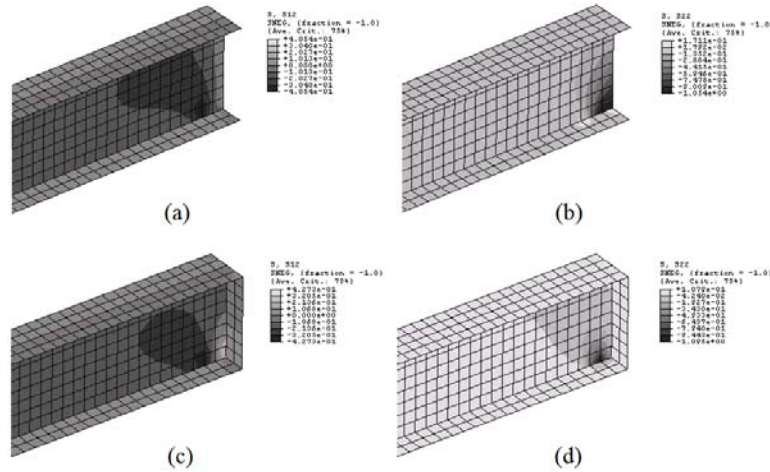beam critical buckling mode, they also change

Fig. 9: (a+c) Shear and (b+d) transverse normal stress distributions near the supports of the unstiffened and stiffened beams (uniformly distributed load)

considerably – the main ones concern modes **7** (*31.4%*), **4** (*24.9%*), **3** (*20.2%*), **10** (*9.7%*), **5** (*7.3%*), **6** (*4.4%*) and **11** (*1.8%*).

(v) As shown above, the transverse extension non-linear term plays a pivotal role, as far as assessing the web-triggered instability of beams acted by transverse loads not applied at the cross-section shear center is concerned. Therefore, GBT models not incorporating this term (to the authors' best knowledge, all the ones developed up to now) may lead to considerably erroneous results when adopted to analyze this type of problems.

(vi) There is again very good agreement between the GBT and ABAQUS critical buckling loads (table 1) and mode shapes (figs. 8(a)-(d)). The P_{cr} differences values are equal to either *1.1%* (unstiffened beam) or *3.9%* (stiffened beam) – concerning the latter, the stiffener modeling explains again the lower value yielded by the GBT analysis.

(vii) Obviously, the support reactions are transmitted distinctly in the stiffened and unstiffened beams. In the latter case, higher and more widespread (vii$_1$) shear and (vii$_2$) compressive transverse normal stresses develop in the web – this can be readily attested by comparing figures 9(a+b) and 9(c+d). Naturally, these stress distributions render the unstiffened beam much more prone to undergo web localized buckling (or web crippling).

I-Section Cantilevers. One analyses now an I-section cantilever (i) with the cross-section and material properties indicated in figure 10(a) and (ii) acted by a tip transverse point load Q causing major axis bending and applied at either the end cross-

section (i) top flange, (ii) shear center or (iii) bottom flange – no nodal displacement and/or rotations is allowed at the fixed end cross-section. Adopting the cross-section discretization shown in figure 10(b), the GBT cross-section analysis leads to a set of *39* deformation modes – the 18 most relevant for the analyses under consideration are displayed in figure 11. As for the longitudinal discretization, it involves *12* finite elements, thus corresponding to a total of *780* degrees of freedom.

First, recall once again that it is essential to include the shear and transverse extension deformation modes in the first-order analysis aimed at determining accurately the pre-buckling stresses, thus capturing all relevant geometrically non-linear effects. Figure 12 shows curves that provide the variation of the cantilever critical buckling moment ($M_{cr}=Q_{cr}L$) with its length (L), for the three tip transverse load locations mentioned above – the modal participation diagrams of the corresponding critical buckling modes are displayed in figure 13. As for figure 14, it depicts the GBT-based critical buckling mode shapes of cantilevers with various lengths and the three tip load locations. The observation of these buckling results prompts the following comments:

(i) The cantilever critical buckling mode may be either lateral-torsional or local-plate (see fig. 14) – the latter may be triggered by the compressed flange (near the fixed end) or the web (near the load application region).
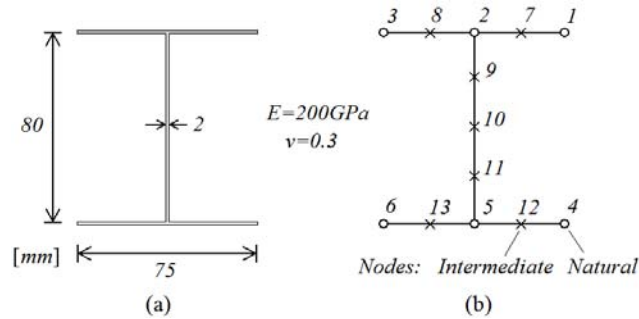

Fig. 10: Cantilever I-section (a) geometry and dimensions and elastic constants, and (b) GBT nodal discretization
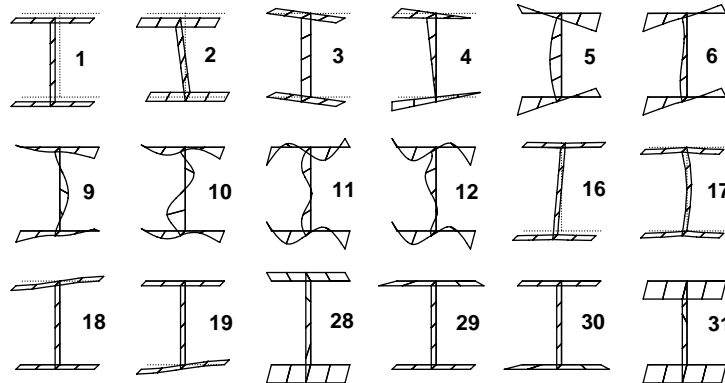
Fig. 11: Most relevant cantilever I-section deformation modes: global (**1**-**4**), local-plate (**5**-**12**), shear (**13**-**21**) and transverse extension (**22**-**30**)

(ii) The flange-triggered local-plate buckling is not affected by the load position. Conversely, the lateral-torsional and web-triggered local-plate buckling phenomena are strongly influenced by this parameter.

(iii) As far as lateral-torsional buckling is concerned, an upward motion of the load point of application (iii$_1$) leads to a M_{cr} decrease and (iii$_2$) causes
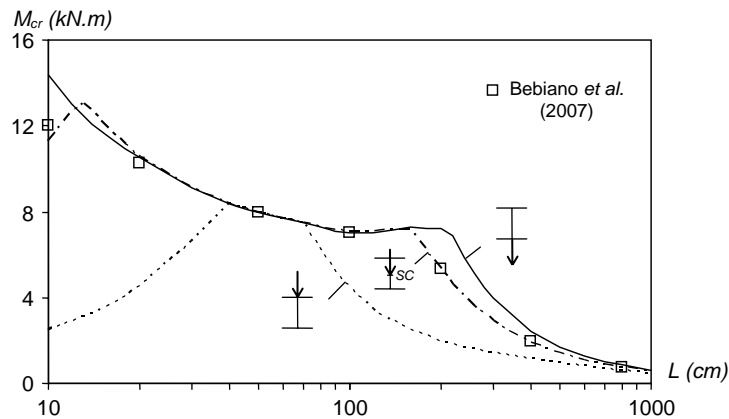

Fig. 12: I-section cantilevers: $M_{cr}(L)$ buckling curves concerning the three positions of the tip point transverse load
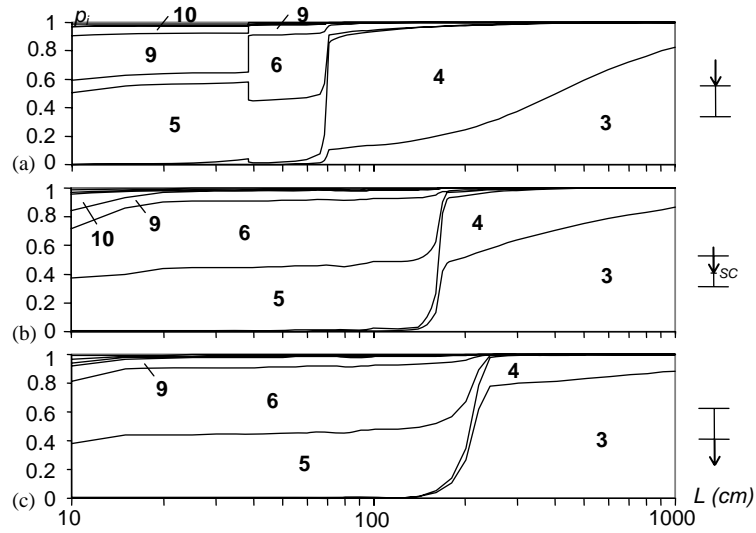
Fig. 13: GBT modal participation diagrams of I-section cantilevers under tip point loads acting at the (a) top flange, (b) shear center and (c) bottom flange
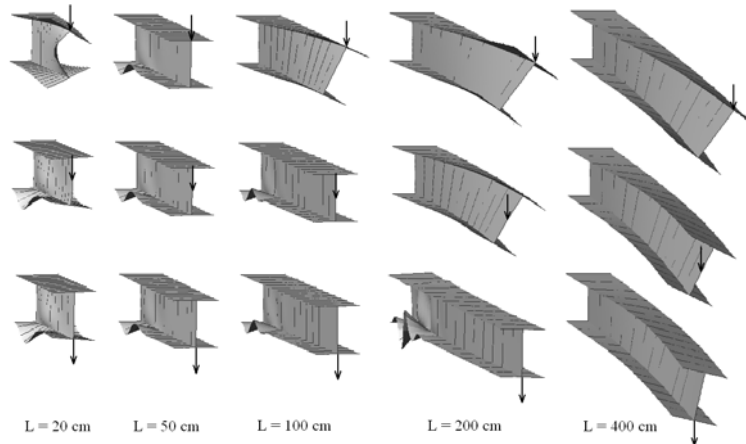

Fig. 14: I-section cantilever: GBT-based critical buckling mode shapes for various lengths and the three load positions under consideration

this buckling phenomenon to be critical for shorter cantilevers. Moreover, the GBT modal participation diagrams presented in figures 13(a)-(c) show clearly that the torsion mode **4** contribution to the lateral-torsional buckling mode decreases as (iii$_1$) L increases (for a given load position) and (iii$_2$) the load position moves downwards (for a given L).

(iv) Besides the expected contributions from the global deformation modes **3** and **4**, the cantilever so-called "lateral-torsional buckling modes" also exhibit small participations from local-plate modes − however, they decrease as the cantilevers become longer (see figs. 13 (a)-(c)). For instance, consider the $L=200$ cm cantilever subjected to shear center loading, for which one has $M_{cr}=5.30$ kN.m and a critical buckling mode combining deformation modes **3** (*51.9%*), **4** (*42.9%*), **5** (*3%*), **9** (*1.3%*) and **6** (*0.8%*) − for top flange loading, M_{cr} drops to *1.99 kN.m* and the modal participations (iv$_1$) increase for modes **4** (*73.6%*) and **6** (*1.9%*), and (iv$_1$) decrease for modes **3** (*24.3%*) and **5** (*0.2%*) and **9** (*0%*).

(v) In cantilevers with lengths comprised between *40 cm* and *70 cm*, the local-plate critical buckling mode is always triggered by the compressed flange near the fixed end, regardless of the load position − since it is applied far away from the region where the instability occurs, the M_{cr} values are exactly the same for the three load positions. For instance, the $L=50$ cm cantilever has $M_{cr}=7.96$ kN.m and a critical buckling mode combining of mostly the local-plate deformations modes **6** (*45.7%*), **5** (*44.2%*) and **9** (*6.9%*) − figures 13 (a)-(c) show clearly that the modal participations do not vary within the *40-70 cm* length range (note that, in the shear center and bottom flange loading cases, the modal participations are exactly the same for $L=40\text{-}160$ cm).

(vi) The cantilevers with $L<40$ cm and subjected to top flange loading buckle in local-plate triggered by the web zone close to the cantilever free end (see fig. 14 − $L=20$ cm). Within this length range, M_{cr} increases with L, because the length increase overshadows the (logical) drop in the critical buckling *load Q_{cr}* (the cantilever becomes more flexible). For $L=20$ cm, one has $Q_{cr}=22.4$ kN ($M_{cr}=4.48$ kN.m) and the critical buckling mode has (vi$_1$) predominant contributions from the symmetric local-plate modes **5** (*55.6%*) and **9** (*28.2%*), and (vi$_2$) lesser participations from modes **6** (*7.6%*), **10** (*5.2%*), **12** (*1.4%*) and **4** (*0.8%*).

(vii)As expected, the M_{cr} (or Q_{cr}) values associated with the shear center loading virtually replicate those recently published by Bebiano *et al.* (2007). Note, however, that the model developed by these authors only includes non-linear terms of the works done by the longitudinal normal and shear stresses, as there is no such term concerning the work done by the transverse normal stresses − this absence precludes the capture of all effects stemming from the load position with respect to the shear center.

Hat-Section Cantilevers. The last illustrative example concerns the buckling behavior of hat-section cantilevers (i) with the geometry and elastic constants given in figure 15(a) and (ii) acted by two identical tip transverse point loads applied at either the web-flange or web-lip corners – the value of each of them is *Q/2* (*i.e.*, *Q* is the total applied load). The adopted GBT cross-section discretization, depicted in figure 15(b), leads to *39* deformation modes – the *18* most relevant ones are displayed in figure 16. Moreover, the longitudinal discretization always involves *8* beam finite elements, leading to a total of 520 degrees of freedom. For validation purposes, one also performs ABAQUS shell finite element analyses – as before (simply supported I-beams), these cantilevers are discretized into fine S9R5 element meshes.

The main objective is to assess the influence of the load position on the cantilever critical buckling moment ($M_{cr}=Q_{cr}.L$) and mode shape. Figures 17, 18 and 19 present, for the two loadings considered, (i) $M_{cr}(L)$ buckling curves, (ii) the corresponding GBT modal participations diagrams and (iii) the GBT-based critical buckling mode shapes of cantilevers with four lengths. The observation of these buckling results leads to the following conclusions:
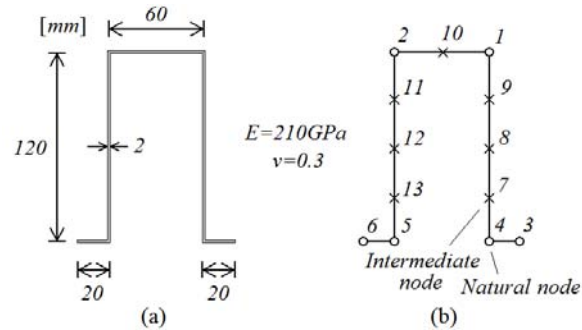

Fig 15: Cantilever hat-section (a) geometry, dimensions and elastic constants, and (b) GBT nodal discretization
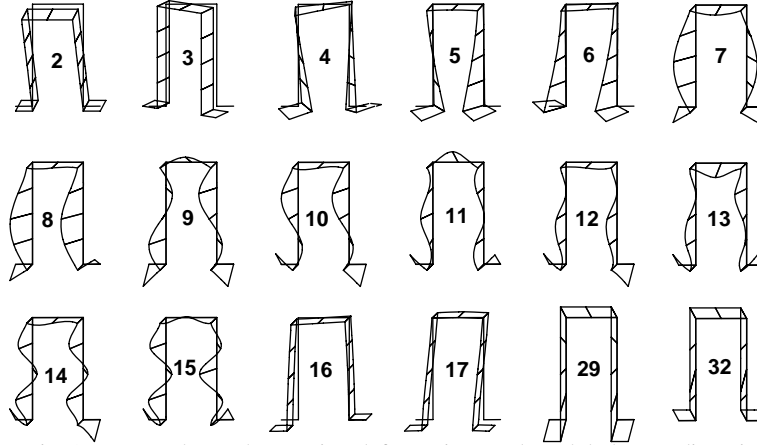
Fig. 16: Most relevant hat-section deformation modes: global (**1-4**), distortional (**5-6**), local-plate (**7-15**), shear (**16-19**) and transverse extension (**28-32**)

(i) There is a very visible difference between the cantilever critical buckling behaviors associated with the two loadings (loads applied at the web-flange and web-lip corners, *i.e.*, top and bottom loading) − M_{cr} values and mode shapes. Concerning the critical buckling moments, the values corresponding to top loading may be more than *40%* lower than their bottom loading counterparts (see fig. 17). In both cases, the critical buckling modes include relevant contributions from global, distortional and local-plate deformation modes, as clearly shown in figures 18 (a)-(b) – they combine (i_1) symmetric distortional (**5**) and local-plate (**7**, **9**, **11**, **13**, **15**) modes, for *L<55 cm*, or (i_2) anti-symmetric global (**3**, **4**), distortional (**6**) and local-plate (**8**, **10**) modes, for *L<55 cm*.

(ii) In order to illustrate the statements made in the previous item, consider the *L=50 cm* and *L=100 cm* cantilevers, associated with the two critical buckling mode types. In the first case, one has (ii_1) M_{cr}=*14.26 kN.m* and critical buckling mode participations from deformation modes **5** (*66.2%*), **7** (*21.9%*), **9** (*7.3%*), **11** (*2%*), **13** (*1.7%*) and **15** (*0.9%*), for top loading, and (ii_2) M_{cr}=*24.65 kN.m* and contributions from modes **7** (*41.6%*), **5** (*27.6%*), **9** (*18.6%*), **13** (*6%*), **11** (*3.0%*) and **15** (*2.5%*), for bottom loading – note the *73%* critical moment increase. In the second

case, one has (ii_1) M_{cr}=*10.67 kN.m* and contributions to the critical buckling mode from deformation modes **4** (*80.2%*), **6** (*15.9%*), **3** (*2.4%*),
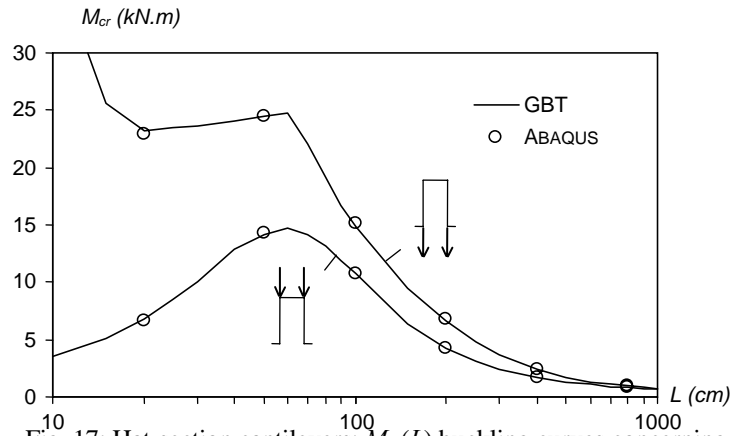
Fig. 17: Hat-section cantilevers: $M_{cr}(L)$ buckling curves concerning the two positions of the tip point loads
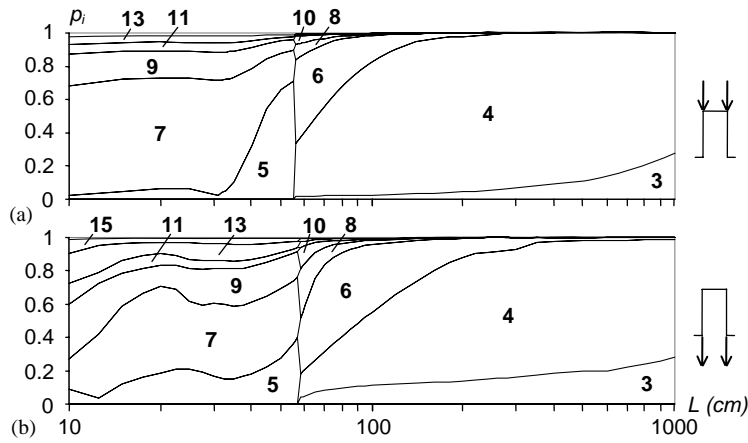

Fig. 18: GBT modal participation diagrams of hat -section cantilevers under (a) top (web-flange corners) and (b) bottom (web-lip corners) tip loading
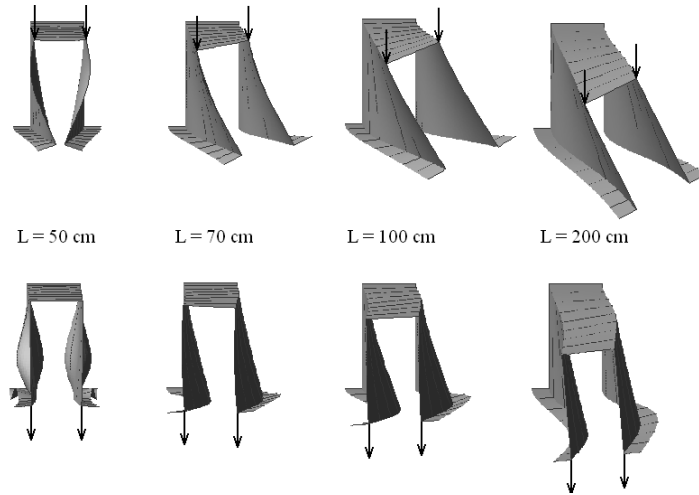
Fig. 19: Hat-section cantilevers: GBT-based critical buckling mode shapes for four lengths and the two loadings under consideration

8 (*0.7%*) and **10** (*0.5%*), for top loading, and (ii₂) *M$_{cr}$=14.84 kN.m* and participations from modes **4** (*43.9%*), **6** (*40.5%*), **3** (*11.2%*), **8** (*2.7%*), **10** (*0.6%*) and **12** (*0.5%*), for bottom loading − now, besides the *39%* critical moment increase, the participation of mode **4** (torsion) decreases, while those of modes **3** (bending) and **6** (distortion) increase (see figs. 18(a)-(b)).

(iii) The comparison between the critical buckling moment provided by the GBT and ABAQUS analyses showed an excellent agreement for all cantilever lengths, as can be readily attested by looking at figure 17 − the differences never exceed *4%*, thus confirming the great accuracy of the GBT analyses (in spite of the small number of d.o.f. involved)[14].

Conclusion

This paper presented a novel GBT formulation that includes a non-linear transverse extension term, thus making it possible to handle rigorously the influence of localized effects on the local (local-plate or distortional) and global buckling behavior of prismatic thin-walled members − in particular, this formulation accounts for effects stemming from (i) the position of transverse loads (with respect to cross-section shear centers) or (ii) the occurrence of localized web buckling phenomena. In order to illustrate the application and potential of the developed and implemented

---

[14] The adopted shell finite element discretizations involve between *120* and *12000* elements (depending on the cantilever length), corresponding to *1250* to *125000* degrees of freedom.

GBT formulation, one presented and discussed numerical results concerning the buckling behavior of (i) hat and I-section cantilevers acted by transverse tip point loads applied at various cross-section points, and (ii) I-section simply supported beams under top-flange distributed and point loads – one also assessed how end support transverse web stiffeners improve the beam buckling behavior. The GBT-based buckling results were validated through the comparison with values yielded by ABAQUS shell finite element analyses (most cases) or reported in the literature. Among the various conclusions drawn from the performance of this work, the following ones deserve a special mention:

(i)   The proposed GBT formulation/implementation was shown to provide accurate buckling results and also to be computationally very efficient (its application always requires a fairly small number of degrees of freedom) – it requires sequentially performing first-order and buckling analyses. Moreover, an excellent agreement was consistently found between the critical buckling loads/moments and mode shapes provided by the GBT and ABAQUS (shell finite element) analyses.

(ii) It is essential to include the transversal extension non-linear term in the GBT analyses intended to study global, local and/or localized wall buckling phenomena caused by transverse loads – the influence of this term becomes particularly noticeable when the load (or support reaction) point of application does not coincide with the cross-section shear center, thus entailing the development of significant (membrane) transverse normal stresses. In one illustrative example addressed in this work, omitting the transverse extension non-linear term from the analyses led to an overestimation of the critical buckling loads/moments that reached *50%* (end stiffened beams) or *300%* (unstiffened beams).

(iii) As expected, the numerical results confirmed the relevance of including web transverse stiffeners at the simply supported I-beam end supports – critical buckling load/moment increases of up to *250%* were observed.

(iv) The GBT modal nature made it possible to acquire more in-depth insight on the mechanics underlying the thin-walled member buckling behavior (through the analysis of the corresponding modal participation diagrams).

Acknowledgements

References

Bradford M.A. (1992). Lateral distortional buckling of steel I-section members, *Journal of Constructional Steel Research*, **23**(1-3), 97-116.

Bebiano R., Silvestre N. and Camotim D. (2007). GBT formulation to analyze the buckling behaviour of thin-walled members under non-uniform bending, *International Journal of Structural Stability and Dynamics*, **7**(1), 23-54.

Camotim D., Silvestre N., Gonçalves R. and Dinis P.B. (2004). GBT analysis of thin-walled members: new formulations and applications, *Thin-Walled Structures: Recent Advances and Future Trends in Thin-Walled Structures Technology* (Loughborough, 25/6), J. Loughlan (ed.), Canopus Publishing Ltd., Bath, 137-168.

Camotim D., Silvestre N., Gonçalves R. and Dinis P.B. (2006a). GBT-based structural analysis of thin-walled members: overview, recent progress and future developments, *Advances in Engineering Structures, Mechanics and Construction* (SMCD 2006 – Waterloo, 14-17/5), M. Pandey, W.C. Xie, L. Xu (eds.), Springer, 187-204.

Camotim D., Silvestre N., Dinis P.B., Bebiano R. and Basaglia C. (2006b). Recent progress in the numerical analysis of thin-walled steel members and frames, *Proceedings of International Symposium on Innovative Design of Steel Structures* (Hong Kong, 10/11), B. Young (ed.), 63-104.

CEN (Comité Européen de Normalisation) (2005), *Eurocode 3: Design of Steel Structures - Part 1.1: General Rules and Rules for Buildings* (EN 1993-1-1), Brussels.

CEN (Comité Européen de Normalisation) (2006), *Eurocode 3: Design of Steel Structures - Part 1.5: Plated Structural Elements* (EN 1993-1-5), Brussels.

Dinis P.B., Gonçalves R. and Camotim D. (2008). On the local and global buckling behaviour of cold-formed steel hollow-flange channel beams, *Proceedings of Fifth International Conference on Thin-Walled Structures* (ICTWS 2008 – Brisbane, 18-20/6). (in press)

Gonçalves R. and Camotim D. (2004). Application of generalised beam theory (GBT) to investigate the local and global stability of cold-formed steel beams, *Computational Methods in Engineering* (CMCE – Lisboa, 31/5-2/6), C.M. Soares *et al.* (eds.), 191. (full paper in CD-ROM Proceedings) (Portuguese)

Gonçalves R. (2007). *Analysis of Thin-Walled Beams with Deformable Cross-Sections: New Formulations and Applications*, PhD thesis in Civil Engineering, IST, Technical University of Lisbon, 2007. (Portuguese)

HKS (Hibbit, Karlsson & Sorensen Inc.) (2002). *Abaqus Standard* (vrs. 6.3-1).

Kumar A. and Samanta A. (2006). Distortional buckling in monosymmetric I-beams: reverse-curvature bending, *Thin-Walled Structures*, **44**(7), 721-725.

Lucic D. and Scepanovic B. (2004). Experimental investigation on locally pressed I-beams subjected to eccentric patch loading, *Journal of Constructional Steel Research*, **60**(3-5), 525-534.

Pi Y.L. and Trahair N.S. (1997). Lateral-distortional buckling of hollow flange beams, *Journal of Structural Engineering* (ASCE), **123**(6), 695-702.

Samanta A. and Kumar A. (2006). Distortional buckling in monosymmetric I-beams, *Thin-Walled Structures*, **44**(1), 51-56.

Silva N.M.F., Camotim D. and Silvestre N. (2008). GBT cross-section analysis of thin-walled members with arbitrary cross-sections: a novel approach, *Proceedings of Fifth International Conference on Thin-Walled Structures* (ICTWS 2008 – Brisbane, 18-20/6). (in press)

Silvestre N. and Camotim D. (2002). First order generalised beam theory for arbitrary orthotropic materials, *Thin-Walled Structures*, **40**(9), 755-789.

Silvestre N. and Camotim D. (2003). GBT buckling analysis of pultruded FRP lipped channel members, *Computers and Structures*, **81**(18-19), 1889-1904.

Topkaya C. (2006). A numerical study on linear bifurcation web buckling of steel I-beams in the sidesway mode, *Engineering Structures*, **28**(7), 1028-1037.

Trahair N.S. (1993). *Flexural-Torsional Buckling of Structures*, E & FN Spon (Chapman & Hall), London.

Turvey G.J. (1996). Effects of load position on the lateral buckling response of pultruded GRP cantilevers – comparisons between theory and experiment, *Composite Structures*, **35**(1), 33-47.